Nighttime atmospheric chemistry of iodine

Alfonso Saiz-Lopez[1], John M.C. Plane[2], Carlos A. Cuevas[1], Anoop S. Mahajan[3], Jean-François Lamarque[4] and Douglas E. Kinnison[4]

[1]Department of Atmospheric Chemistry and Climate, Institute of Physical Chemistry Rocasolano, CSIC, Madrid, Spain

[2]School of Chemistry, University of Leeds, Leeds, UK

[3]Indian Institute of Tropical Meteorology, Pune, India

[4]Atmospheric Chemistry Observations and Modelling, NCAR, Colorado, USA

Correspondence to: A. Saiz-Lopez (a.saiz@csic.es)

1   **Abstract**

2   Little attention has so far been paid to the nighttime atmospheric chemistry of iodine species.

3   Current atmospheric models predict a buildup of HOI and I_2 during the night that leads to a spike

4   of IO at sunrise, which is not observed by measurements. In this work, electronic structure

5   calculations are used to survey possible reactions that HOI and I_2 could undergo at night in the

6   lower troposphere, and hence reduce their nighttime accumulation. The new reaction NO_3 + HOI

7   → IO + HNO_3 is proposed, with a rate coefficient calculated from statistical rate theory over the

8   temperature range 260 - 300 K and at a pressure of 1000 hPa to be $k(T) = 2.7$ x 10^{-12} (300 K / T

9    $)^{2.66}$ cm^3 molecule^{-1} s^{-1}. This reaction is included in two atmospheric models, along with the

10   known reaction between I_2 and NO_3, to explore a new nocturnal iodine radical activation

11   mechanism. The results show that this iodine scheme leads to a considerable reduction of

12   nighttime HOI and I_2, which results in the enhancement of more than 25% of nighttime ocean

13   emissions of HOI + I_2 and the removal of the anomalous spike of IO at sunrise. We suggest that

14   active nighttime iodine can also have a considerable, so far unrecognized, impact on the

15   reduction of the NO_3 radical levels in the marine boundary layer (MBL) and hence upon the

16   nocturnal oxidizing capacity of the marine atmosphere. The effect of this is exemplified by the

17   indirect effect on dimethyl sulfide (DMS) oxidation.

1. Introduction

Active nighttime iodine chemistry was first evidenced a decade ago when it was shown that nocturnal I_2 emitted by macroalgae could react with NO_3 leading to the formation of IO and OIO, which were measured in the coastal MBL at Mace Head, Ireland (Saiz-Lopez and Plane, 2004). The nitrate radical has also been recently suggested as a nocturnal loss of CH_2I_2, which helps to reconcile observed and modelled concentrations of this iodocarbon over the remote MBL (Carpenter et al., 2015). However, most of the work on reactive atmospheric iodine has focused on the use of daytime observations and models to assess its role in the catalytic destruction of ozone and the oxidizing capacity of the troposphere (e.g. Saiz-Lopez et al. (2012b) and references therein). In the MBL, iodine-, along with bromine-catalysed ozone destruction contributes up to 45% of the observed daytime depletion (Read et al., 2008; Mahajan et al., 2010a), although this contribution shows large geographical variability (Mahajan et al., 2012; Gómez Martín et al., 2013; Prados-Roman et al., 2015b; Volkamer et al., 2015). Iodine compounds have also been implicated in the formation of aerosols, although the mechanisms and magnitudes of these processes are not fully understood (Hoffmann et al., 2001; O'Dowd et al., 2002; McFiggans et al., 2004; Gomez Martin et al., 2013; Allan et al., 2015; Roscoe et al., 2015). Reactive forms of inorganic iodine may also contribute to the oxidation of elemental mercury over the tropical oceans (Wang et al., 2014). In recent years, iodine sources and chemistry have also been implemented in global models demonstrating the effect of iodine chemistry in the oxidation capacity of the global marine troposphere (Ordóñez et al., 2012; Saiz-Lopez et al., 2012a; Saiz-Lopez et al., 2014; Sherwen et al., 2016).

Iodine is emitted into the atmosphere from the ocean surface in both organic and inorganic forms. The main organic compounds emitted are methyl iodide (CH_3I), ethyl iodide (C_2H_5I),

1   propyl iodide (1- and 2-C_3H_7I), chloroiodomethane (CH_2ICl), bromoiodomethane (CH_2IBr), and

2   diiodomethane (CH_2I_2) (Carpenter, 2003; Butler et al., 2007; Jones et al., 2010; Mahajan et al.,

3   2012). However, these organic compounds contribute only up to a fourth of the MBL iodine

4   loading (Jones et al., 2010; Mahajan et al., 2010a; Großmann et al., 2013; Prados-Roman et al.,

5   2015b). Inorganic emissions of HOI and I_2, which result from the deposition of O_3 at the ocean

6   surface and subsequent reaction with I^- ions in the surface microlayer, account for the main

7   source of iodine in the MBL (Carpenter et al., 2013). Recent laboratory experiments have shown

8   that HOI is the major compound emitted, and provided parameterizations of the fluxes of both

9   species depending on wind speed, temperature, and the concentrations of O_3 and I^- (Carpenter et

10   al., 2013; MacDonald et al., 2014). These parameterized fluxes of HOI and I_2 have then been

11   used in a one-dimensional model to study the diurnal evolution of the IO and I_2 mixing ratios at

12   the Cape Verde Atmospheric Observatory (CVAO) (Carpenter et al., 2013; Lawler et al., 2014).

13   The model simulations replicate well the levels and general diurnal profiles of IO and I_2,

14   although an early morning 'dawn spike' in IO is predicted by the models, but has not been

15   observed   (Read et al., 2008; Mahajan et al., 2010a). The morning peak predicted by current

16   iodine chemistry models is due to a buildup of the emitted I_2 and HOI (which is converted into

17   IBr/ICl through heterogeneous sea-salt recycling) over the course of the night, followed by rapid

18   photolysis at sunrise.

19   Traditionally it has been thought that iodine chemistry has a negligible effect on oxidizing

20   capacity of the nocturnal marine atmosphere. As a consequence, unlike the demonstrated effect

21   of iodine on the levels of daytime oxidants, the impact of active iodine upon the main nighttime

22   oxidant, NO_3, remains an open question. This is important given that in many parts of the ocean

23   the NO_3 + DMS reaction is at least as important as OH + DMS in oxidizing DMS (Allan et al.,

1 2000), and hence a reduction of NO_3 may have an effect in the production of SO_2 and methane

2 sulfonic acid (MSA). Here, we discuss possible mechanisms of nighttime iodine radical

3 activation and their potential effect on nighttime iodine ocean fluxes and the currently modeled

4 dawn spike in IO. A new reaction of HOI with NO_3 is proposed, supported by theoretical

5 calculations. We explore the implications of this new reaction both for iodine and NO_3

6 chemistries.

8 **2. Nocturnal iodine radical activation mechanism**

9 We use the reaction mechanism that has recently been described in the global modelling studies

10 by Saiz-Lopez et al. (2014) and (Ordóñez et al., 2012) (see supplementary information). In

11 addition to the reactions included in that scheme, we also include nighttime gas-phase reactions

12 based on the theoretical calculations described below. The additional reactions are listed in Table

13 1 and a scheme with this new nocturnal chemistry is included in Figure 1.

14 To the best of our knowledge, reactions of HOI specific to night time have not been studied,

15 either theoretically or through laboratory experiments. Currently, HOI is thought to build up

16 overnight until sunrise, with only heterogeneous uptake on seasalt aerosol as a nighttime loss

17 process (Saiz-Lopez et al., 2012b; Simpson et al., 2015). In addition to the well known $I_2 + NO_3$

18 reaction (R1) (Chambers et al., 1992), here we consider several possible HOI reactions that could

19 occur at night, in the absence of photolysis and OH:

20 $\qquad HOI + NO_2 \rightarrow I + HNO_3$ (R2)

21 $\qquad HOI + HNO_3 \rightarrow IONO_2 + H_2O$ (R3)

1      $HOI + NO_3 \rightarrow IO + HNO_3$ (R4)

3   **3. Theoretical calculations**

4   In order to explore the feasibility of reactions 2–4 taking place under the conditions of the lower

5   troposphere, we carried out electronic structure calculations using the hybrid density

6   functional/Hartree-Fock B3LYP method from within the Gaussian 09 suite of programs (Frisch

7   et al., 2009), combined with a G2 level basis set for I (Glukhovtsev et al., 1995) and the standard

8   6-311+g(2d,p) triple zeta basis set for O, N and H. Following geometry optimizations of the

9   relevant points on the potential energy surfaces, and the determination of their corresponding

10   vibrational frequencies and (harmonic) zero-point energies, energies relative to the reactants

11   were obtained at the same level of theory. Spin-orbit corrections of -30.0 (Mečiarová et al.,

12   2011), -14.4 (Khanniche et al., 2016), -5.9 (Šulková et al., 2013) and -4.8 (Kaltsoyannis and

13   Plane, 2008) kJ mol^{-1} were applied to the energies of I , IO, HOI and $IONO_2$, respectively.

14   Reaction 2 is endothermic by 2.6 kJ mol^{-1} and so, within the expected error of ±10 kJ mol^{-1} at

15   this level of theory, might be reasonably fast. However, the transition state of the reaction, which

16   is illustrated in Figure 2(a), is 73 kJ mol^{-1} above the reactants and so this reaction will not occur

17   at tropospheric temperatures. Reaction 3 is exothermic by 19.8 kJ mol^{-1}. An $HOI\text{--}HNO_3$

18   complex first forms (Figure 2(b)), which is 21 kJ mol^{-1} below the reactants. However, this

19   complex re-arranges to the $IONO_2 + H_2O$ products via the cyclic transition state shown in Figure

20   2(c), which is 110 kJ mol^{-1} above the reactants.

21   The stationary points on the potential energy surface (PES) for reaction 4 are illustrated in Figure

22   3. HOI and NO_3 associate to form a complex which is 24 kJ mol^{-1} below the reactant entrance

channel. H-atom transfer involves a submerged transition state to form an IO--HNO$_3$ complex, which can then dissociate to the products IO + HNO$_3$. The vibrational frequencies, rotational energies and geometries (in Cartesian co-ordinates) of these intermediates are listed in Table 2. Overall, the reaction is exothermic by 14 kJ mol^{-1}. The energies of the HOI--NO$_3$ complex and the transition state are assigned the same spin-orbit correction as HOI (-5.9 kJ mol^{-1} (Šulková et al., 2013)), whereas the IO--HNO$_3$ complex is assigned the spin-orbit correction of IO (-14.4 kJ mol^{-1} (Khanniche et al., 2016)). This reflects the H-OI bond only increasing from 0.97 Å in HOI to 1.1 Å in the transition state, compared with 1.7 Å in the IO—HNO$_3$ complex. The spin-orbit correction for the transition state is therefore likely to be closer to that of HOI. Assigning the HOI spin-orbit correction therefore means that the barrier is highest with respect to the reactants, so that the estimated rate coefficient (see below) may be a lower limit.

The rate coefficient for reaction 4 was then estimated using Rice-Ramsperger-Kassel-Markus (RRKM) theory, employing a multi-well energy-grained master equation solver based on the inverse Laplace transform method - MESMER (Master Equation Solver for Multi-well Energy Reactions) (Roberston et al., 2014). The reaction proceeds via the formation of the excited HOI--NO$_3$ complex from HOI + NO$_3$. This complex can then dissociate back to the reactants or rearrange to the IO--HNO$_3$ intermediate complex over the transition state, which can in turn dissociate to the products IO + HNO$_3$. Either of the intermediates can also be stabilized by collision with the third body (N$_2$). The time evolution of all these possible outcomes is modelled using the master equation.

The internal energies of the intermediates on the PES were divided into a contiguous set of grains (width 10 cm^{-1}), each containing a bundle of rovibrational states calculated with the molecular parameters in Table 2, using the rigid-rotor harmonic oscillator approximation for all

1   species. It should be noted that the HOI--NO$_3$ and IO--HNO$_3$ complexes both have low

2   frequency vibrational modes (< 100 cm^{-1}) which should more correctly be treated as hindered

3   rotors rather than vibrations. However, in our experience this is not worth doing this until

4   experimental rate coefficients are available to fit the rotor barrier heights. In any case, the

5   energies of both complexes are far enough below the energy of the entrance channel (figure 3)

6   that relatively small changes in their densities of states will have a minor effect on the overall

7   rate coefficient. Each grain was then assigned a set of microcanonical rate coefficients linking it

8   to other intermediates, calculated by RRKM theory. For dissociation to products or reactants,

9   microcanonical rate coefficients were determined using inverse Laplace transformation to link

10   them directly to the capture rate coefficient, $k_{capture}$. For reaction 4 and the reverse reaction IO +

11   HNO$_3$ involving neutral species, $k_{capture}$ was set to a typical capture rate coefficient of 2.5×10^{-10}

12   $(T/300$ K$)^{1/6}$ cm^3 molecule^{-1} s^{-1}, where the small positive temperature dependence is

13   characteristic of a long-range potential governed by dispersion and   dipole-dipole forces

14   (Georgievskii and Klippenstein, 2005).

15   The probability of collisional transfer between grains was estimated using the exponential down

16   model, where the average energy for downward transitions was set to $<\Delta E>_{down} = 300$ cm^{-1} for

17   N$_2$ as the third body (Gilbert and Smith, 1990). MESMER determines the temperature- and

18   pressure-dependent rate coefficient from the full microcanonical description of the system time

19   evolution by performing an eigenvector/eigenvalue analysis (Bartis and Widom, 1974). The

20   resulting rate coefficient over the temperature range 260 - 300 K at a pressure of 1000 hPa is

21   $k_4(T) = 2.7 \times 10^{-12}$ (300 K / T)$^{2.66}$ cm^3 molecule^{-1} s^{-1}. Because the intermediate complexes are

22   not strongly bound, and the transition state and products are below the entrance channel, the only

23   products formed in reaction R4 under atmospheric conditions are IO + HNO$_3$. The uncertainty in

1 k_4 arises principally from the estimated capture rate coefficient (see above), and the height of the

2 barrier below the entrance channel. As discussed above, the spin-orbit correction of the transition

3 state is likely to be larger than the value of -5.9 kJ mol^{-1} corresponding to HOI, so k_4 is possibly a

4 lower limit. For instance, if the barrier height is decreased by 3 kJ mol^{-1}, k_4 increases by a factor

5 of 1.9. If the barrier is lower by 8.5 kJ mol^{-1} (corresponding to the transition state having the

6 same spin-orbit correction as IO), then k_4 would increase by a factor of 5.1. Nevertheless, noting

7 that the capture rate coefficient could be lower – perhaps by a factor of 2 - than the estimate used

8 here, we prefer to use the value for k_4 calculated with the potential surface in Figure 3. Of course,

9 if k_4 is larger, then the atmospheric impacts of reaction 4 discussed in Section 4 will be even

10 more pronounced.

11 Note that NO_3 also reacts with CH_2I_2 with a rate constant $\sim$2-4$\times$10^{-13} cm^3 molecule^{-1} s^{-1}, which

12 can have a significant effect on nighttime CH_2I_2 concentration (Carpenter et al., 2015). However

13 the products of this reaction are still uncertain (Nakano et al., 2006; Carpenter et al., 2015) and

14 its rate is considerably slower than that of R4.

15 In summary, the only likely gas-phase reactions that I_2 and HOI undergo in the nighttime

16 troposphere are R1 and R4, respectively. These are included in the model reaction scheme to

17 examine their impacts on the evolution of iodine species in the atmosphere.

19 **4. Atmospheric modelling**

20 We use two atmospheric chemical transport models to study i) the impact of this new chemistry

21 on the nighttime chemistry and partitioning of iodine species, and ii) the resulting geographical

22 distribution of nocturnal iodine and impact on NO_3 within the global marine boundary layer.

1   The first model, Tropospheric HAlogen chemistry MOdel (THAMO), is used for a detailed

2   kinetics study of the impact of the different reactions shown in Table 1 as well as to assess which

3   uptake rates best reproduce observations from a field study at the CVAO (Carpenter et al., 2011).

4   THAMO has been used in the past to study iodine chemistry at the CVAO and further details

5   including the full chemical scheme can be found elsewhere (Read et al., 2008; Saiz-Lopez et al.,

6   2008; Mahajan et al., 2009; Mahajan et al., 2010a; Mahajan et al., 2010b; Lawler et al., 2014).

7   Briefly, THAMO is a 1-D chemistry transport model with 200 stacked boxes at a vertical

8   resolution of 5m (total height 1 km). The model treats iodine, bromine, O_3, NO_x and HO_x

9   chemistry, and is constrained with typical measured values of other chemical species in the

10   MBL: [CO]=110 nmol mol^{-1}; [DMS]=30 pmol/mol; [CH4]=1820 nmol mol^{-1};[ethane]=925

11   pmol/mol; [CH3CHO]=970 pmol/mol; [HCHO]=500 pmol/mol; [isoprene]=10 pmol/mol;

12   [propane]=60 pmol/mol; [propene]=20 pmol/mol. The average background aerosol surface area

13   (ASA) used is $1x10^{-6}$ cm^2 cm^{-3} (Read et al., 2008; Lee et al., 2009; Read et al., 2009; Lee et al.,

14   2010). The model is initialized at midnight and the evolution of iodine species, O_3, NO_x and HO_x

15   is followed until the model reaches steady state.

16   The second model is the global 3D chemistry-climate model CAM-Chem (Community

17   Atmospheric Model with chemistry, version 4.0), which is used to study the impact of reactions

18   1 and 4 on a global scale. The model includes a comprehensive chemistry scheme to simulate the

19   evolution of trace gases and aerosols in the troposphere and the stratosphere (Lamarque et al.,

20   2012). The model runs with the iodine and bromine chemistry schemes from previous studies

21   (Fernandez et al., 2014; Saiz-Lopez et al., 2014; Saiz-Lopez et al., 2015), including the

22   photochemical breakdown of bromo- and iodo-carbons emitted from the oceans (Ordóñez et al.,

23   2012) and abiotic oceanic sources of HOI and I_2 (Prados-Roman et al., 2015a). CAM-Chem has

1   been configured in this work with a horizontal resolution of 1.9º latitude by 2.5º longitude and 26

2   vertical levels, from the surface to ~40km altitude. All model runs in this study were performed

3   in the specified dynamics mode (Lamarque et al., 2012) using offline meteorological fields

4   instead of an online calculation, to allow direct comparisons between different simulations. This

5   offline meteorology consists of a high frequency meteorological input from a previous free

6   running climatic simulation.

7   It should be noted that during nighttime the uptake on aerosols of emitted species such as I_2 and

8   HOI, and the uptake of reservoir species such as $IONO_2$, can play a major role in the cycling of

9   iodine. Observations at CVAO show that I_2 peaked at about 1 pmol/mol during the night and that

10   ICl was not detected above the 1 pmol/mol detection limit of the instrument (Lawler et al.,

11   2014). In order to match these observations, we need to reduce the uptake and heterogeneous

12   recycling of iodine species. The uptake rates of chemical species on the background seasalt

13   aerosols are determined by their uptake coefficients (γ). The database of mass accommodation

14   and/or uptake coefficients is rather sparse and essentially limited to I_2, HI, HOI, ICl, IBr on pure

15   water/ice and on sulphuric acid particles (Sander et al., 2006). Other iodine species which are

16   likely to undergo uptake onto aerosol are OIO, HIO_3, INO_2, $IONO_2$, I_2O_2 (Saiz-Lopez et al.,

17   2012a; Sommariva et al., 2012). Uptake of HOI is very uncertain, with γ(HOI) ranging from 2 $\times$

18   10^{-3} to 0.3 depending on the surface composition and state (Holmes et al., 2001). Sommariva et

19   al. (2012) assumed γ(HOI) to be 0.6, similar to the value for HOBr measured by Wachsmuth et

20   al. (2002). In the case of $IONO_2$, the uptake coefficient has not been measured, with most models

21   using values of 0.1 (von Glasow et al., 2002; Saiz-Lopez et al., 2008; Mahajan et al., 2009; Leigh

22   et al., 2010; Mahajan et al., 2010a; Mahajan et al., 2010b; Sommariva et al., 2012; Lawler et al.,

23   2014). The modelled levels of I_2 and ICl change with different values of uptake coefficients. To

1   match the CVAO I_2 and ICl observations (Lawler et al., 2014), we have used $\gamma = 0.01$ for HOI

2   and $IONO_2$, which is within the uncertainty in the literature, and assumed that 80% is recycled as

3   I_2. Further measurements of these dihalogen species are needed to better constrain their

4   heterogeneous recycling on seasalt aerosols.

6   5. Results and discussion

7   Of the possible nocturnal iodine activation reactions involving the inorganic iodine source gases

8   I_2 and HOI, only reactions R1 and R4 appear to be likely candidates (see Section 3). We

9   therefore designed two modelling scenarios: Scenario 1 (S1), without nighttime reactions of I_2 or

10   HOI with NO_3; and Scenario 2 (S2), including reactions R1 and R4 for the degradation of HOI

11   and I_2 by NO_3. In the one-dimensional model THAMO, the I_2 and HOI are injected into the

12   atmosphere from the ocean surface using the flux parameterizations derived from laboratory

13   experiments (Carpenter et al., 2013; MacDonald et al., 2014). Figure 4 shows the resulting

14   diurnal evolution of the HOI and I_2 mixing ratios in the two scenarios, after two days of

15   simulation time. The I_2 mixing ratio peaks during the night in both the scenarios due to quick

16   loss by photolysis during the daytime. By contrast, HOI is present during daytime due to its

17   production through the reaction of IO with HO_2, and peaks just before sunset. In the first

18   scenario, without the inclusion of reactions R1 and R4, Figure 4 (right-hand side panels) shows

19   that I_2 builds up during the night, reaching a concentration peak just before dawn. This is

20   especially noticeable as the daytime concentrations are much lower than during the night. On the

21   other hand, HOI concentrations decrease during night until dawn, when they drop to zero. For

22   both species, inclusion of reactions with NO_3 causes a decrease in their respective nocturnal

1   concentrations (Fig. 4, left-hand side panels). The inclusion of reactions R1 and R4 also leads to

2   a modelled I_2 concentration which is in better agreement with the observations of the molecule

3   made at CVAO (Lawler et al., 2014), reaching peak values of about 1 pmol/mol, as compared to

4   about 3 pmol/mol for the scenario without nighttime reactions. An additional consequence of

5   including reactions R1 and R4 is the significant increase of the sea-air fluxes of HOI and I_2 at

6   night due to their atmospheric removal by NO_3 (Fig. 4, bottom panel).

7   Figure 5 shows the diurnal evolution of IO, NO_3 and $IONO_2$ in both model scenarios after two

8   days of simulation time. Although the daytime peak values of IO are well reproduced in both

9   scenarios, reaching about 1.5 pmol/mol around noon similar to the ground-based observations

10   (Read et al., 2008), the inclusion of reactions R1 and R4 leads to the removal of the dawn spike

11   in IO, which is predicted by current iodine models but was not observed at CVAO (Read et al.,

12   2008; Mahajan et al., 2010a) . The IO dawn spike predicted by models is due to a buildup of the

13   emitted I_2 and HOI (which is converted into IBr/ICl through heterogeneous recycling) over the

14   night, followed by rapid photolysis after first sunlight. However, due to the considerable removal

15   of HOI and I_2 through the night due to reaction with ambient NO_3, this spike does not appear in

16   the second scenario, leading to a modification of the diurnal profile of IO that better matches

17   with observations.

18   Reactions R1 and R4 also reduce the NO_3 mixing ratio (Fig. 5, middle panels). In scenario 1, the

19   NO_3 is modelled to peak at about 14 pmol/mol just before dawn. However, the inclusion of

20   reactions R1 and R4 leads to near complete depletion of NO_3 close to the surface, with the peak

21   level at the surface reaching only 2 pmol/mol, since reactions R1 and R4 become the main

22   atmospheric loss processes for NO_3 in the lower MBL. These reactions lead however to the

23   buildup of $IONO_2$ during the night (Fig. 5, bottom panels). In the absence of reactions R1 and

1   R4, significant levels of $IONO_2$ are seen only at dawn and dusk since no other reactions produce

2    $IONO_2$ at night, and during the day $IONO_2$ is removed by photolysis. However, with continuous

3   conversion of I_2 and HOI to $IONO_2$ by reactions R1 and R4 in scenario 2, $IONO_2$ is modelled to

4   reach up to 3 pmol/mol in the nocturnal MBL.

5   Given the associated uncertainty in the theoretical estimate of the k_4, we used THAMO to assess

6   the sensitivity of surface NO_3 to k_4. Figure 6 shows that NO_3 peak nighttime concentration is in

7   fact highly coupled to k_4, with the expected uncertainty in k_4 of one order of magnitude (see

8   above) giving rise to a factor of two change in NO_3. A laboratory measurement of $k4$ should

9   therefore be undertaken in the future.

10   We now implement the nighttime reactions in the 3D global model (CAM-Chem) to assess the

11   resulting geographical distributions and impacts of these reactions. We have also run two

12   different scenarios in CAM-Chem, the first without R1 and R4 in the chemical scheme, and the

13   second including the new nighttime iodine chemistry. Figure 7 shows how the inclusion of R1

14   and R4 reduces globally the nighttime concentrations of I_2 and HOI. The plots correspond to the

15   nighttime averaged (from 00LT to 01LT (Local Time)) differences between the model scenarios.

16   Considerable reductions of up to 0.5 and 10 pmol/mol (i.e. up to 100% removal) are observed for

17   I_2 and HOI, respectively, particularly over coastal polluted regions where continental pollution

18   outflow leads to higher levels of NO_3 in the nighttime MBL. Major shipping routes also show

19   strong nocturnal iodine activity due to the characteristically high NO_x, and resulting NO_3,

20   associated with shipping emissions.

21   Figure 8 shows the effect of this nocturnal chemistry on the concentrations of $IONO_2$ and NO_3.

22   As in the previous figure, the plots correspond to the nighttime averaged difference between the

second and the first scenarios. The maps show an increase of $IONO_2$ of up to 15 pmol/mol

(~600%) over polluted coastal areas, due to efficient conversion of NO_3 into $IONO_2$. The bottom

panel of Figure 7 shows the expected decrease of NO_3 levels associated with the inclusion of

reactions R1 and R4, with decreases of up to ~4 pmol/mol (up to 60%) over marine polluted

regions. We model global percentage reductions in the NO_3 concentrations of 7.1% (60S-60N),

with nitrate removal of up to 80% in non-polluted remote oceanic regions with low NO_3 levels.

This in turn can affect the modelled oxidation of DMS by NO_3. We estimate that the reduction in

NO_3, due to the inclusion of R1 and R4, results in a model increase in DMS levels of up to 7

pmol/mol (about 20%) in marine regions affected by continental pollution outflow (Fig. 9). We

therefore suggest that the inclusion of the new nighttime iodine chemistry can have a large, so far

unrecognized, impact on the nocturnal oxidizing capacity of the marine atmosphere.

The hourly evolution of the main species involved in this study is shown in Figures 10 and 11,

which include the levels of HOI, I_2, $IONO_2$ and NO_3 in the MBL over regions where nocturnal

iodine is modelled to be particularly active. The first region is located within the Mediterranean

Sea, an area that shows large differences during the summer months when high ozone levels

drive large emissions of HOI and I_2 from the sea, and the high levels of NO_3 at nighttime make

this chemistry especially important. The hourly average in August is shown in Figure 10 for

HOI, $IONO_2$ and I_2. HOI and $IONO_2$ (Fig 10) are the species whose concentration differ most

between scenarios as HOI is removed and $IONO_2$ produced by R4 (and, to a lesser extent, R1).

Over a Pacific Ocean region at the south of the Baja California Peninsula, the modelled

differences between the two scenarios are even higher than over the Mediterranean Sea (Figure

11). Large differences in MBL NO_3, up to 28%, are modelled during the night caused by

pollution outflow from the west coasts of Mexico and USA.

6. Summary and conclusions

3 The viability of the reaction of HOI with NO_2, HNO_3 and NO_3 has been studied by theoretical

4 calculations. The results indicate that only the reaction of HOI with NO_3, to yield IO + HNO_3, is

5 possible under tropospheric conditions. The inclusion of this reaction, along with that of I_2 +

6 NO_3, has a number of significant implications: *i*) nocturnal iodine radical chemistry is activated;

7 *ii*) this causes enhanced nighttime oceanic emissions of HOI and I_2; *iii*) nighttime iodine species

8 are partitioned into high levels of $IONO_2$; *iv*) the IO spike, modelled by current iodine models

9 but not shown by observations, is removed; and, *v*) a reduction of the levels of nitrate radical in

10 the MBL, with the associated less efficient oxidation of DMS, which has important implications

11 for our understanding of the nocturnal oxidizing capacity of the marine atmosphere.

14 **Acknowledgments**

15 This work was supported by the Spanish National Research Council (CSIC). The National

16 Center for Atmospheric Research (NCAR) is funded by the National Science Foundation NSF.

17 The Climate Simulation Laboratory at NCAR's Computational and Information Systems

18 Laboratory (CISL) provided the computing resources (ark:/85065/d7wd3xhc). As part of the

19 CESM project, CAM-Chem is supported by the NSF and the Office of Science (BER) of the US

20 Department of Energy. This work was also sponsored by the NASA Atmospheric Composition

21 Modeling and Analysis Program Activities (ACMAP, number NNX11AH90G).

2 **References**

3 Allan, B. J., McFiggans, G., Plane, J. M. C., Coe, H., and McFadyen, G. G.: The nitrate radical

4 in the remote marine boundary layer, Journal of Geophysical Research: Atmospheres, 105,

5 24191-24204, 10.1029/2000jd900314, 2000.

6 Allan, J. D., Williams, P. I., Najera, J., Whitehead, J. D., Flynn, M. J., Taylor, J. W., Liu, D.,

7 Darbyshire, E., Carpenter, L. J., Chance, R., Andrews, S. J., Hackenberg, S. C., and McFiggans,

8 G.: Iodine observed in new particle formation events in the Arctic atmosphere during

9 ACCACIA, Atmos. Chem. Phys., 15, 5599-5609, 10.5194/acp-15-5599-2015, 2015.

10 Bartis, J. T., and Widom, B.: Stochastic models of the interconversion of three or more chemical

11 species, J. Chem. Phys., 60, 3474-3482, doi: 10.1063/1.1681562, 1974.

12 Butler, J. H., King, D. B., Lobert, J. M., Montzka, S. A., Yvon-Lewis, S. A., Hall, B. D.,

13 Warwick, N. J., Mondeel, D. J., Aydin, M., and Elkins, J. W.: Oceanic distributions and

14 emissions of short-lived halocarbons, Global Biogeochem. Cycles, 21, GB1023,

15 10.1029/2006gb002732, 2007.

16 Carpenter, L. J.: Iodine In the marine Boundary Layer, Chem. Rev., 103 (12), 4953-4962, 2003.

17 Carpenter, L. J., Fleming, Z. L., Read, K. A., Lee, J. D., Moller, S. J., Hopkins, J. R., Purvis, R.

18 M., Lewis, A. C., Müller, K., Heinold, B., Herrmann, H., Fomba, K. W., Pinxteren, D., Müller,

19 C., Tegen, I., Wiedensohler, A., Müller, T., Niedermeier, N., Achterberg, E. P., Patey, M. D.,

20 Kozlova, E. A., Heimann, M., Heard, D. E., Plane, J. M. C., Mahajan, A., Oetjen, H., Ingham, T.,

21 Stone, D., Whalley, L. K., Evans, M. J., Pilling, M. J., Leigh, R. J., Monks, P. S., Karunaharan,

A., Vaughan, S., Arnold, S. R., Tschritter, J., Pöhler, D., Frieß, U., Holla, R., Mendes, L. M., Lopez, H., Faria, B., Manning, A. J., and Wallace, D. W. R.: Seasonal characteristics of tropical marine boundary layer air measured at the Cape Verde Atmospheric Observatory, J. Atmos. Chem., 67, 87-140, 10.1007/s10874-011-9206-1, 2011.

Carpenter, L. J., MacDonald, S. M., Shaw, M. D., Kumar, R., Saunders, R. W., Parthipan, R., Wilson, J., and Plane, J. M. C.: Atmospheric iodine levels influenced by sea surface emissions of inorganic iodine, Nature Geosci, 6, 108-111, 10.1038/ngeo1687, 2013.

Carpenter, L. J., Andrews, S. J., Lidster, R. T., Saiz-Lopez, A., Fernandez-Sanchez, M., Bloss, W. J., Ouyang, B., and Jones, R. L.: A nocturnal atmospheric loss of CH2I2 in the remote marine boundary layer, J. Atmos. Chem., 10.1007/s10874-015-9320-6, 2015.

Fernandez, R. P., Salawitch, R. J., Kinnison, D. E., Lamarque, J. F., and Saiz-Lopez, A.: Bromine partitioning in the tropical tropopause layer: implications for stratospheric injection, Atmos. Chem. Phys., 14, 13391-13410, 10.5194/acp-14-13391-2014, 2014.

Frisch, M., Trucks, G., Schlegel, H., Scuseria, G., Robb, M., Cheeseman, J., Scalmani, G., Barone, V., Mennucci, B., and Petersson, G.: Gaussian 09, Revision A. 1. Wallingford, CT: Gaussian, in, Inc, 2009.

Georgievskii, Y., and Klippenstein, S. J.: Long-range transition state theory, J. Chem. Phys., 122, 194103, doi: 10.1063/1.1899603, 2005.

Gilbert, R. G., and Smith, S. C.: Theory of Unimolecular and Recombination Reactions, Blackwell, Oxford, 1990.

1 Glukhovtsev, M. N., Pross, A., McGrath, M. P., and Radom, L.: Extension of Gaussian-2 (G2)

2 theory to bromine- and iodine-containing molecules: Use of effective core potentials, J. Chem.

3 Phys., 103, 1878-1885, 1995.

4 Gomez Martin, J. C., Galvez, O., Baeza-Romero, M. T., Ingham, T., Plane, J. M. C., and Blitz,

5 M. A.: On the mechanism of iodine oxide particle formation, Phys. Chem. Chem. Phys., 15,

6 15612-15622, 10.1039/c3cp51217g, 2013.

7 Gómez Martín, J. C., Mahajan, A. S., Hay, T. D., Prados-Román, C., Ordóñez, C., MacDonald,

8 S. M., Plane, J. M. C., Sorribas, M., Gil, M., Paredes Mora, J. F., Agama Reyes, M. V., Oram, D.

9 E., Leedham, E., and Saiz-Lopez, A.: Iodine chemistry in the eastern Pacific marine boundary

10 layer, Journal of Geophysical Research: Atmospheres, 118, 887-904, 10.1002/jgrd.50132, 2013.

11 Großmann, K., Frieß, U., Peters, E., Wittrock, F., Lampel, J., Yilmaz, S., Tschritter, J.,

12 Sommariva, R., von Glasow, R., Quack, B., Krüger, K., Pfeilsticker, K., and Platt, U.: Iodine

13 monoxide in the Western Pacific marine boundary layer, Atmos. Chem. Phys., 13, 3363-3378,

14 10.5194/acp-13-3363-2013, 2013.

15 Hoffmann, T., O'Dowd, C. D., and Seinfeld, J. H.: Iodine oxide homogeneous nucleation: An

16 explanation for coastal new particle production, Geophys. Res. Lett., 28, 1949-1952, 2001.

17 Holmes, N. S., Adams, J. W., and Crowley, J. N.: Uptake and reaction of HOI and IONO2 on

18 frozen and dry NaCl/NaBr surfaces and H2SO4, Phys. Chem. Chem. Phys., 3, 1679-1687,

19 10.1039/b100247n, 2001.

1   Jones, C. E., Hornsby, K. E., Sommariva, R., Dunk, R. M., von Glasow, R., McFiggans, G., and

2   Carpenter, L. J.: Quantifying the contribution of marine organic gases to atmospheric iodine,

3   Geophys. Res. Lett., 37, L18804, 2010.

4   Kaltsoyannis, N., and Plane, J. M. C.: Quantum chemical calculations on a selection of iodine-

5   containing species (IO, OIO, INO_3, $(IO)_2$, I_2O_3, I_2O_4 and I_2O_5) of importance in the atmosphere.,

6   Phys. Chem. Chem. Phys., 10, 1723-1733, 2008.

7   Khanniche, S., Louis, F., Cantrel, L., and Černušák, I.: A Density Functional Theory and ab

8   Initio Investigation of the Oxidation Reaction of CO by IO Radicals, J. Phys. Chem. A, 120,

9   1737−1749, 2016.

10   Lamarque, J. F., Emmons, L. K., Hess, P. G., Kinnison, D. E., Tilmes, S., Vitt, F., Heald, C. L.,

11   Holland, E. A., Lauritzen, P. H., Neu, J., Orlando, J. J., Rasch, P. J., and Tyndall, G. K.: CAM-

12   chem: description and evaluation of interactive atmospheric chemistry in the Community Earth

13   System Model, Geosci. Model Dev., 5, 369-411, 10.5194/gmd-5-369-2012, 2012.

14   Lawler, M. J., Mahajan, A. S., Saiz-Lopez, A., and Saltzman, E. S.: Observations of I2 at a

15   remote marine site, Atmos. Chem. Phys., 14, 2669-2678, 10.5194/acp-14-2669-2014, 2014.

16   Lee, J. D., Moller, S. J., Read, K. A., Lewis, A. C., Mendes, L., and Carpenter, L. J.: Year-round

17   measurements of nitrogen oxides and ozone in the tropical North Atlantic marine boundary layer,

18   Journal of Geophysical Research: Atmospheres, 114, n/a-n/a, 10.1029/2009jd011878, 2009.

19   Lee, J. D., McFiggans, G., Allan, J. D., Baker, A. R., Ball, S. M., Benton, A. K., Carpenter, L. J.,

20   Commane, R., Finley, B. D., Evans, M., Fuentes, E., Furneaux, K., Goddard, A., Good, N.,

21   Hamilton, J. F., Heard, D. E., Herrmann, H., Hollingsworth, A., Hopkins, J. R., Ingham, T.,

1 Irwin, M., Jones, C. E., Jones, R. L., Keene, W. C., Lawler, M. J., Lehmann, S., Lewis, A. C.,

2 Long, M. S., Mahajan, A., Methven, J., Moller, S. J., Müller, K., Müller, T., Niedermeier, N.,

3 O'Doherty, S., Oetjen, H., Plane, J. M. C., Pszenny, A. A. P., Read, K. A., Saiz-Lopez, A.,

4 Saltzman, E. S., Sander, R., von Glasow, R., Whalley, L., Wiedensohler, A., and Young, D.:

5 Reactive Halogens in the Marine Boundary Layer (RHaMBLe): the tropical North Atlantic

6 experiments, Atmos. Chem. Phys., 10, 1031-1055, 10.5194/acp-10-1031-2010, 2010.

7 Leigh, R. J., Ball, S. M., Whitehead, J., Leblanc, C., Shillings, A. J. L., Mahajan, A. S., Oetjen,

8 H., Dorsey, J. R., Gallagher, M., Jones, R. L., Plane, J. M. C., Potin, P., and McFiggans, G.:

9 Measurements and modelling of molecular iodine emissions, transport and photodestruction in

10 the coastal region around Roscoff, Atmos. Chem. Phys., 10, 11823-11838, 2010.

11 MacDonald, S. M., Gómez Martín, J. C., Chance, R., Warriner, S., Saiz-Lopez, A., Carpenter, L.

12 J., and Plane, J. M. C.: A laboratory characterisation of inorganic iodine emissions from the sea

13 surface: dependence on oceanic variables and parameterisation for global modelling, Atmos.

14 Chem. Phys., 14, 5841-5852, 10.5194/acp-14-5841-2014, 2014.

15 Mahajan, A. S., Oetjen, H., Saiz-Lopez, A., Lee, J. D., McFiggans, G. B., and Plane, J. M. C.:

16 Reactive iodine species in a semi-polluted environment, Geophys. Res. Lett., 36, L16803,

17 doi:16810.11029/12009GL038018, 2009.

18 Mahajan, A. S., Plane, J. M. C., Oetjen, H., Mendes, L., Saunders, R. W., Saiz-Lopez, A., Jones,

19 C. E., Carpenter, L. J., and McFiggans, G. B.: Measurement and modelling of tropospheric

20 reactive halogen species over the tropical Atlantic Ocean, Atmos. Chem. Phys., 10, 4611-4624,

21 2010a.

1   Mahajan, A. S., Shaw, M., Oetjen, H., Hornsby, K. E., Carpenter, L. J., Kaleschke, L., Tian-

2   Kunze, X., Lee, J. D., Moller, S. J., Edwards, P., Commane, R., Ingham, T., Heard, D. E., and

3   Plane, J. M. C.: Evidence of reactive iodine chemistry in the Arctic boundary layer,, J. Geophys.

4   Res., [Atmos.], 115, D20303, doi:10.1029/2009JD013665, 2010b.

5   Mahajan, A. S., Gómez Martín, J. C., Hay, T. D., Royer, S. J., Yvon-Lewis, S., Liu, Y., Hu, L.,

6   Prados-Roman, C., Ordóñez, C., Plane, J. M. C., and Saiz-Lopez, A.: Latitudinal distribution of

7   reactive iodine in the Eastern Pacific and its link to open ocean sources, Atmos. Chem. Phys., 12,

8   11609-11617, 10.5194/acp-12-11609-2012, 2012.

9   McFiggans, G., Coe, H., Burgess, R., Allan, J., Cubison, M., Alfarra, M. R., Saunders, R., Saiz-

10   Lopez, A., Plane, J. M. C., Wevill, D. J., Carpenter, L. J., Rickard, A. R., and Monks, P. S.:

11   Direct evidence for coastal iodine particles from Laminaria macroalgae - linkage to emissions of

12   molecular iodine, Atmos. Chem. Phys., 4, 701-713, 2004.

13   Mečiarová, K., Šulka, M., Canneaux, S., Louis, F., and Černušáka, I.: A theoretical study of the

14   kinetics of the forward and reverse reactions $HI + CH_3 = I + CH_4$, Chem. Phys. Lett., 517, 149-

15   154, 2011.

16   Nakano, Y., Ukeguchi, H., and Ishiwata, T.: Rate constant of the reaction of NO3 with CH2I2

17   measured with use of cavity ring-down spectroscopy, Chem. Phys. Lett., 430, 235-239, doi:

18   10.1016/j.cplett.2006.09.002, 2006.

19   O'Dowd, C. D., Jimenez, J. L., Bahreini, R., Flagan, R. C., Seinfeld, J. H., Hameri, K., Pirjola,

20   L., Kulmala, M., Jennings, S. G., and Hoffmann, T.: Marine aerosol formation from biogenic

21   iodine emissions, Nature, 417, 632-636, 2002.

1 Ordóñez, C., Lamarque, J. F., Tilmes, S., Kinnison, D. E., Atlas, E. L., Blake, D. R., Sousa

2 Santos, G., Brasseur, G., and Saiz-Lopez, A.: Bromine and iodine chemistry in a global

3 chemistry-climate model: description and evaluation of very short-lived oceanic sources, Atmos.

4 Chem. Phys., 12, 1423-1447, 10.5194/acp-12-1423-2012, 2012.

5 Prados-Roman, C., Cuevas, C. A., Fernandez, R. P., Kinnison, D. E., Lamarque, J. F., and Saiz-

6 Lopez, A.: A negative feedback between anthropogenic ozone pollution and enhanced ocean

7 emissions of iodine, Atmos. Chem. Phys., 15, 2215-2224, 10.5194/acp-15-2215-2015, 2015a.

8 Prados-Roman, C., Cuevas, C. A., Hay, T., Fernandez, R. P., Mahajan, A. S., Royer, S. J., Galí,

9 M., Simó, R., Dachs, J., Großmann, K., Kinnison, D. E., Lamarque, J. F., and Saiz-Lopez, A.:

10 Iodine oxide in the global marine boundary layer, Atmos. Chem. Phys., 15, 583-593,

11 10.5194/acp-15-583-2015, 2015b.

12 Read, K. A., Mahajan, A. S., Carpenter, L. J., Evans, M. J., Faria, B. V. E., Heard, D. E.,

13 Hopkins, J. R., Lee, J. D., Moller, S. J., Lewis, A. C., Mendes, L., McQuaid, J. B., Oetjen, H.,

14 Saiz-Lopez, A., Pilling, M. J., and Plane, J. M. C.: Extensive halogen-mediated ozone

15 destruction over the tropical Atlantic Ocean, Nature, 453, 1232-1235, 2008.

16 Read, K. A., Lee, J. D., Lewis, A. C., Moller, S. J., Mendes, L., and Carpenter, L. J.: Intra-annual

17 cycles of NMVOC in the tropical marine boundary layer and their use for interpreting seasonal

18 variability in CO, Journal of Geophysical Research: Atmospheres, 114, n/a-n/a,

19 10.1029/2009jd011879, 2009.

20 Roberston, S. H., Glowacki, D. R., Liang, C. H., Morley, C., Shannon, R., Blitz, M., and Pilling,

21 M. J.: MESMER (Master Equation Solver for Multi-Energy Well Reactions), 2008–2012: An

1 object oriented C++ program for carrying out ME calculations and eigenvalue-eigenvector

2 analysis on arbitrary multiple well systems, edited. [Available at

3 http://sourceforge.net/projects/mesmer.], in, 4.1 ed., 2014.

4 Roscoe, H. K., Jones, A. E., Brough, N., Weller, R., Saiz-Lopez, A., Mahajan, A. S.,

5 Schoenhardt, A., Burrows, J. P., and Fleming, Z. L.: Particles and iodine compounds in coastal

6 Antarctica, Journal of Geophysical Research: Atmospheres, 120, 7144-7156,

7 10.1002/2015jd023301, 2015.

8 Saiz-Lopez, A., and Plane, J. M. C.: Novel iodine chemistry in the marine boundary layer,

9 Geophys. Res. Lett., 31, L04112, 2004.

10 Saiz-Lopez, A., Plane, J. M. C., Mahajan, A. S., Anderson, P. S., Bauguitte, S. J.-B., Jones, A.

11 E., Roscoe, H. K., Salmon, R. A., Bloss, W. J., Lee, J. D., and Heard, D. E.: On the vertical

12 distribution of boundary layer halogens over coastal Antarctica: implications for O_3, HO_x, NO_x

13 and the Hg lifetime, Atmos. Chem. Phys., 8, 887-900, 2008.

14 Saiz-Lopez, A., Lamarque, J.-F., Kinnison, D., Tilmes, S., Ordóñez, C., Orlando, J. J., Conley,

15 A. J., Plane, J. M. C., Mahajan, A., Sousa Santos, G., Atlas, E., Blake, D. R., Sander, S. P.,

16 Schauffler, S. M., Thompson, A. M., and Brasseur, G.: Estimating the climate significance of

17 halogen-driven ozone loss in the tropical marine troposphere, Atmos. Chem. Phys., 12, 3939-

18 3949, 2012a.

19 Saiz-Lopez, A., Plane, J. M. C., Baker, A. R., Carpenter, L. J., Von Glasow, R., Gómez Martín,

20 J. C., McFiggans, G., and Saunders, R. W.: Atmospheric Chemistry of Iodine, Chem. Rev.

21 (Washington, DC, U. S.), 112, 1773-1804, 10.1021/cr200029u, 2012b.

1 Saiz-Lopez, A., Fernandez, R. P., Ordóñez, C., Kinnison, D. E., Gómez Martín, J. C., Lamarque,

2 J. F., and Tilmes, S.: Iodine chemistry in the troposphere and its effect on ozone, Atmos. Chem.

3 Phys., 14, 13119-13143, 10.5194/acp-14-13119-2014, 2014.

4 Saiz-Lopez, A., Baidar, S., Cuevas, C. A., Koenig, T. K., Fernandez, R. P., Dix, B., Kinnison, D.

5 E., Lamarque, J. F., Rodriguez-Lloveras, X., Campos, T. L., and Volkamer, R.: Injection of

6 iodine to the stratosphere, Geophys. Res. Lett., n/a-n/a, 10.1002/2015gl064796, 2015.

7 Sander, S. P., Orkin, V. L., Kurylo, M. J., Golden, D. M., Huie, R. E., Kolb, C. E., Finlayson-

8 Pitts, B. J., Molina, M. J., Friedl, R. R., Ravishankara, A. R., Moortgat, G. K., Keller-Rudek, H.,

9 and Wine, P. H.: Chemical kinetics and photochemical data for use in atmospheric studies, JPL-

10 NASA, 2006.

11 Sherwen, T., Evans, M. J., Carpenter, L. J., Andrews, S. J., Lidster, R. T., Dix, B., Koenig, T. K.,

12 Sinreich, R., Ortega, I., Volkamer, R., Saiz-Lopez, A., Prados-Roman, C., Mahajan, A. S., and

13 Ordóñez, C.: Iodine's impact on tropospheric oxidants: a global model study in GEOS-Chem,

14 Atmos. Chem. Phys., 16, 1161-1186, 10.5194/acp-16-1161-2016, 2016.

15 Simpson, W. R., Brown, S. S., Saiz-Lopez, A., Thornton, J. A., and Glasow, R. v.: Tropospheric

16 Halogen Chemistry: Sources, Cycling, and Impacts, Chem. Rev., 115, 4035-4062,

17 10.1021/cr5006638, 2015.

18 Sommariva, R., Bloss, W. J., and von Glasow, R.: Uncertainties in gas-phase atmospheric iodine

19 chemistry, Atmos. Environ., 57, 219-232, doi: 10.1016/j.atmosenv.2012.04.032, 2012.

1 Šulková, K., Šulka, M., Louis, F., and Neogrády, P.: Atmospheric Reactivity of CH$_2$ICl with OH

2 Radicals: High-Level OVOS CCSD(T) Calculations for the X‑Abstraction Pathways (X = H, Cl,

3 or I), J. Phys. Chem. A, 117, 771−782, 2013.

4 Volkamer, R., Baidar, S., Campos, T. L., Coburn, S., DiGangi, J. P., Dix, B., Eloranta, E. W.,

5 Koenig, T. K., Morley, B., Ortega, I., Pierce, B. R., Reeves, M., Sinreich, R., Wang, S., Zondlo,

6 M. A., and Romashkin, P. A.: Aircraft measurements of BrO, IO, glyoxal, NO2, H2O, O2–O2

7 and aerosol extinction profiles in the tropics: comparison with aircraft-/ship-based in situ and

8 lidar measurements, Atmos. Meas. Tech., 8, 2121-2148, 10.5194/amt-8-2121-2015, 2015.

9 von Glasow, R., Sander, R., Bott, A., and Crutzen, P. J.: Modeling halogen chemistry in the

10 marine boundary layer. 1. Cloud-free MBL, J. Geophys. Res., 107, 4341, 2002.

11 Wachsmuth, M., Gäggeler, H. W., von Glasow, R., and Ammann, M.: Accommodation

12 coefficient of HOBr on deliquescent sodium bromide aerosol particles, Atmos. Chem. Phys., 2,

13 121-131, 10.5194/acp-2-121-2002, 2002.

14 Wang, F., Saiz-Lopez, A., Mahajan, A. S., Gómez Martín, J. C., Armstrong, D., Lemes, M., Hay,

15 T., and Prados-Roman, C.: Enhanced production of oxidised mercury over the tropical Pacific

16 Ocean: a key missing oxidation pathway, Atmos. Chem. Phys., 14, 1323-1335, 10.5194/acp-14-

17 1323-2014, 2014.

1   **Tables**

3   Table 1: Night time reactions of emitted inorganic iodine compounds considered in addition to
4   the iodine chemistry scheme used by (Saiz-Lopez et al., 2014).

No.	Reaction	Notes
R1.	$I_2 + NO_3 \rightarrow I + IONO_2$	1.5×10^{-12} cm^3 molecule^{-1} s^{-1} [*Chambers et al.*, 1992]
R2.	$HOI + NO_2 \rightarrow I + HNO_3$	Endothermic by 9 kJ mol^{-1} and the transition state is 73 kJ mol^{-1} above the reactants
R3.	$HOI + HNO_3 \rightarrow IONO_2 + H_2O$	Exothermic by 11 kJ mol^{-1}. The reaction first forms a complex 21 kJ mol^{-1} below the reactants but this rearranges to the products via a transition state that is 110 kJ mol^{-1} above the reactants.
R4.	$HOI + NO_3 \rightarrow IO + HNO_3$	Exothermic by 11 kJ mol^{-1} with all transition states below the reactants. $k(T) = 2.7 \times 10^{-12} (300\ K\ /\ T)^{2.66}$ cm^3 molecule^{-1} s^{-1}

1 **Table 2.** Calculated vibrational frequencies, rotational constants and energies of the stationary

2 points and asymptotes on the HOI + NO$_3$ doublet potential energy surface

Species	Geometry[a]	Vibrational frequencies[b]	Rotational constants [c]	Potential energy [d]
HOI + NO$_3$		603, 1084, 3803 & 261, 261, 805,1108, 1108, 1126	623.9, 8.182, 8.076 & 13.84, 13.84, 6.919	0.0
IOH-NO$_3$ complex	O 1.623,0.284,-0.331 H 1.484,-0.657,-0.043 I 0.009,1.205,0.286 N -0.456,-2.265,0.030 O -1.052, -3.321,-0.0473 O -1.147,-1.195,-0.228 O 0.742,-2.161,0.333	55, 84, 118, 161, 196, 615, 629, 667, 705, 803, 968, 1228, 1273,1491, 3268	5.610, 0.916, 0.806	-24.0
IO-H-NO$_2$ TS	O 0.309,1.515,0.247 H -0.834,1.314,-0.017 I 1.280,-0.089,-0.093 N -2.349,-0.133,0.019 O -3.518, ,-0.429,-0.035 O -1.444,-0.962,0.257 O -2.019,1.117,-0.187	1249i, 70, 97, 103, 225, 472, 676, 698, 797, 806, 1041, 1147, 1308, 1513, 1626	6.300, 0.864, 0.767	-16.4
IO-HNO$_3$ complex	O 0.571,1.350,0.348 H -1.111,1.098,-0.020 I 1.870,0.0645,-0.152 N -2.503,-0.202,0.0186 O -3.673,-0.396,-0.170 O -1.654,-0.986,0.401 O -2.081,1.090,-0.242	35, 43, 76, 126, 198, 623, 677, 703, 772, 798, 939, 1331, 1416, 1713, 3281	7.058, 0.605, 0.566	-34.8
IO + HNO$_3$		648 & 477, 585, 649, 782, 901, 1320, 1345, 1738, 3724	9.844 & 13.01, 12.05, 6.258	-10.6

3 [a] Cartesian co-ordinates in Å. [b] Given as wavenumber in cm^{-1}. [c] In GHz. [d] In kJ mol^{-1}, including zero-
4 point energy and spin-orbit coupling of I and IO (see text).
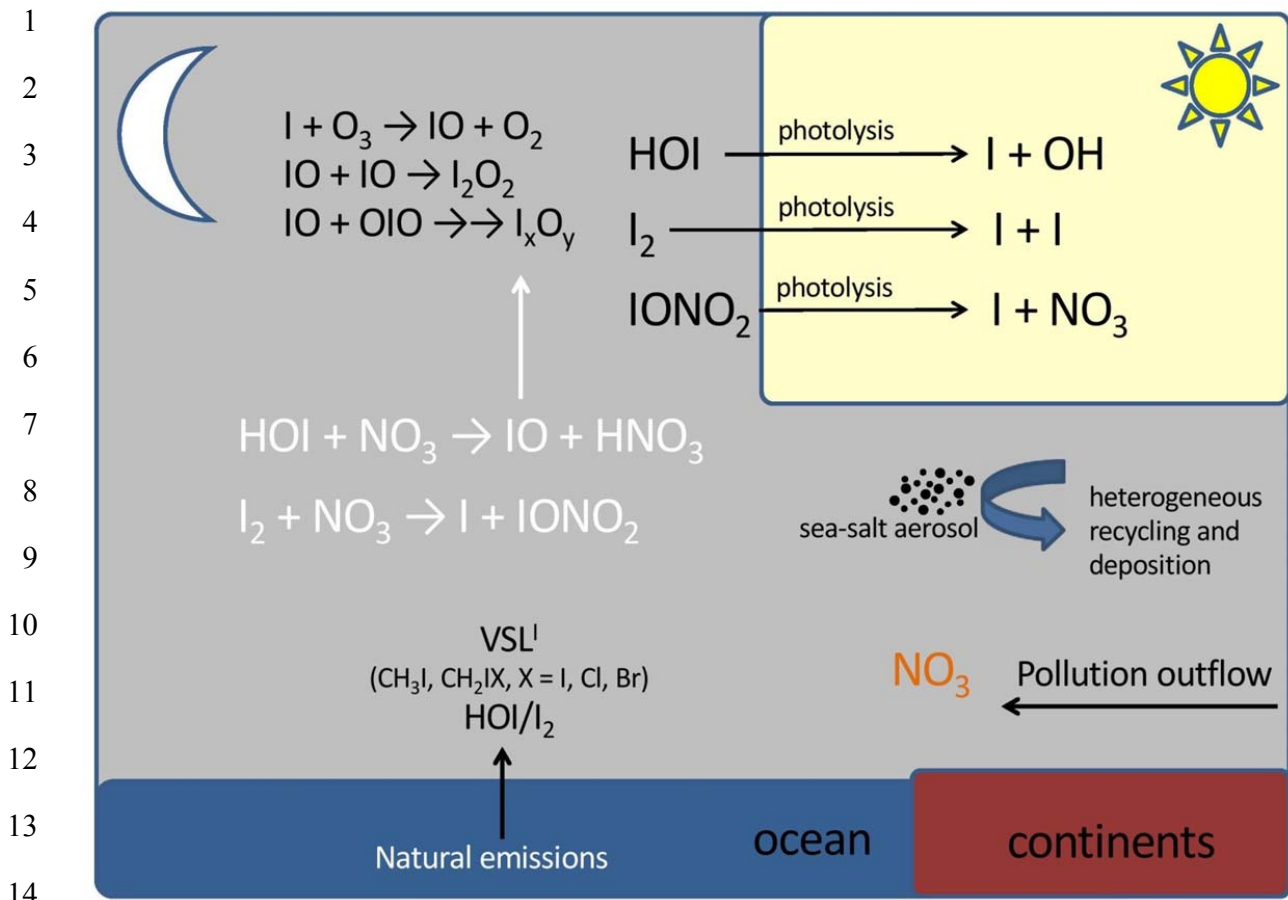
Figure 1. New nocturnal iodine chemistry (in white) implemented in the THAMO and CAM-Chem models.
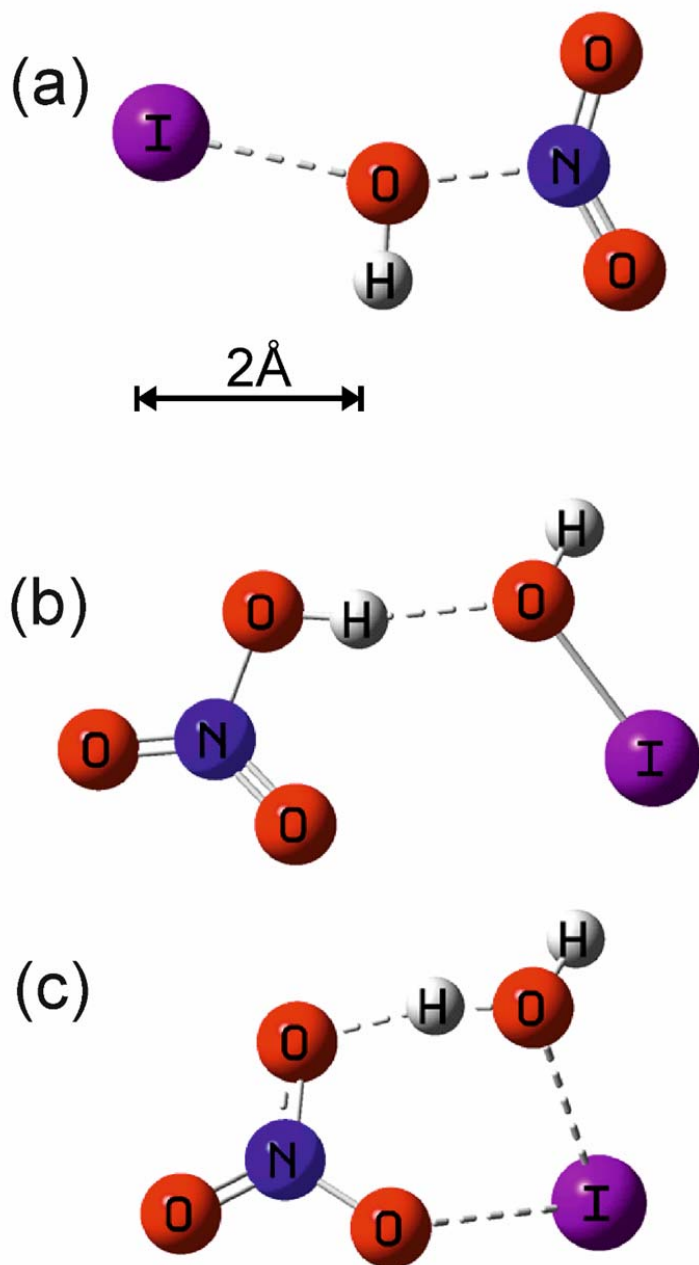
Figure 2: (a) Transition state for the reaction between HOI and NO_2 to form HNO_3 + I; (b) complex formed between HOI and HNO_3, which then reacts via transition state (c) to form $IONO2$ + H_2O.
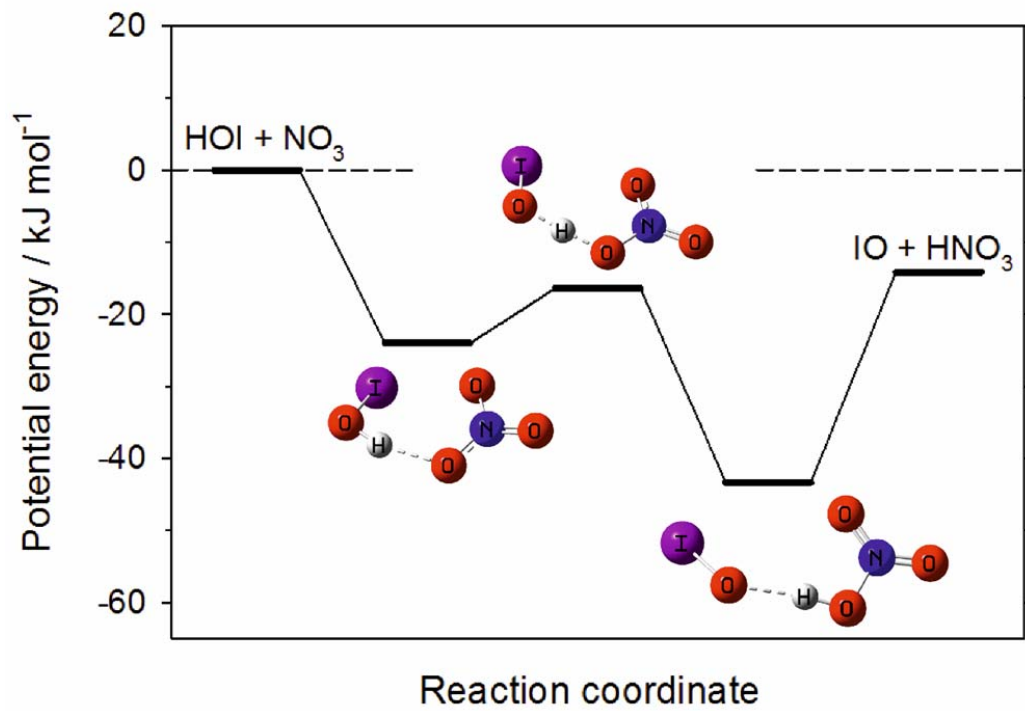
Figure 3. Potential energy surface for the reaction between HOI and NO_3, which contains two intermediate complexes separated by a submerged barrier.
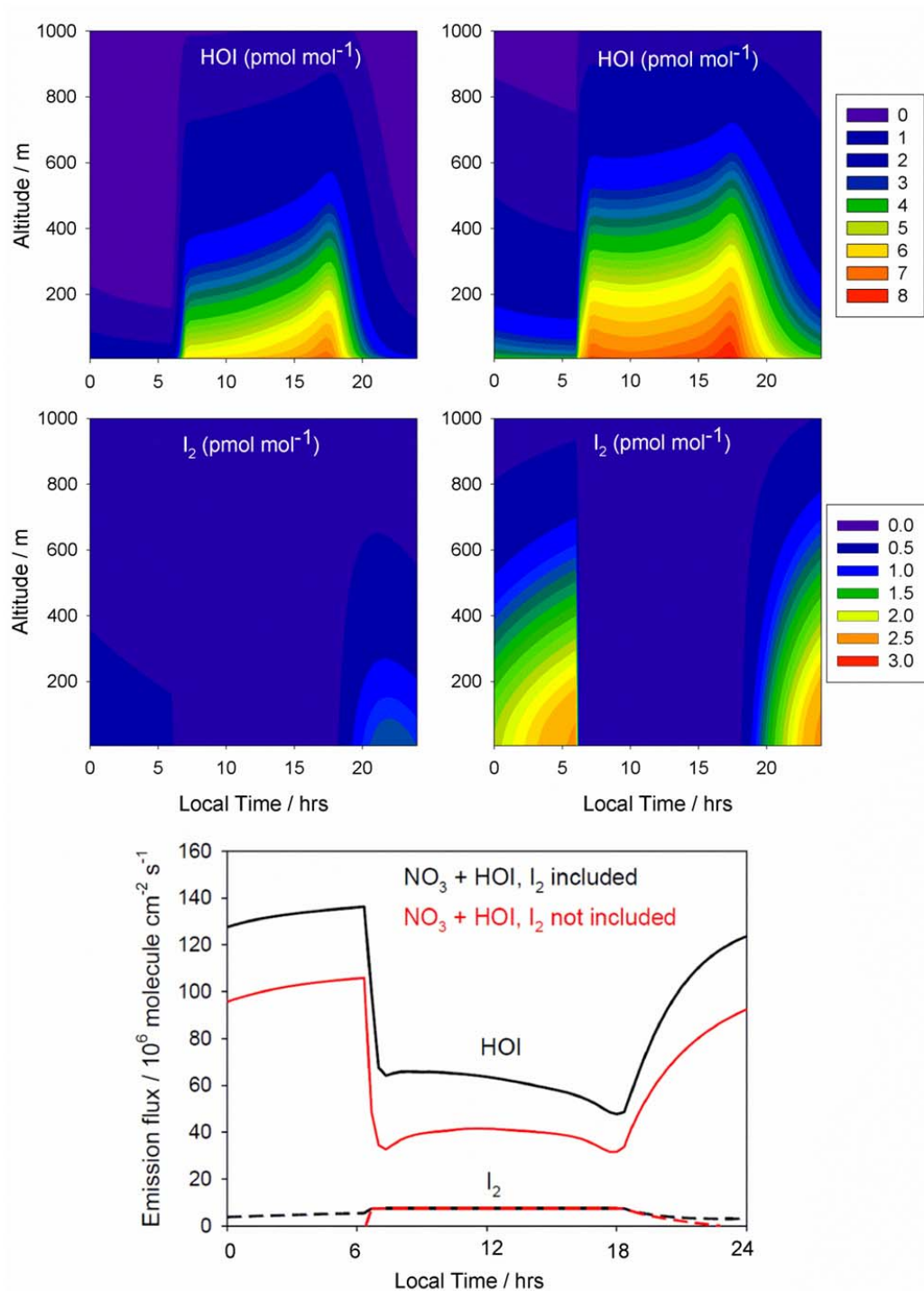
Figure 4. THAMO modeled diurnal variation of HOI, I_2 (upper panels) and the HOI/I_2 flux from
the ocean surface (bottom panel). The right hand panels are from scenario 1, which do not
include night time reactions of HOI and I_2 with NO_3, while the left hand panels include the
reactions in scenario 2. In bottom panel red lines represent scenario 1, while black lines
correspond to scenario 2.
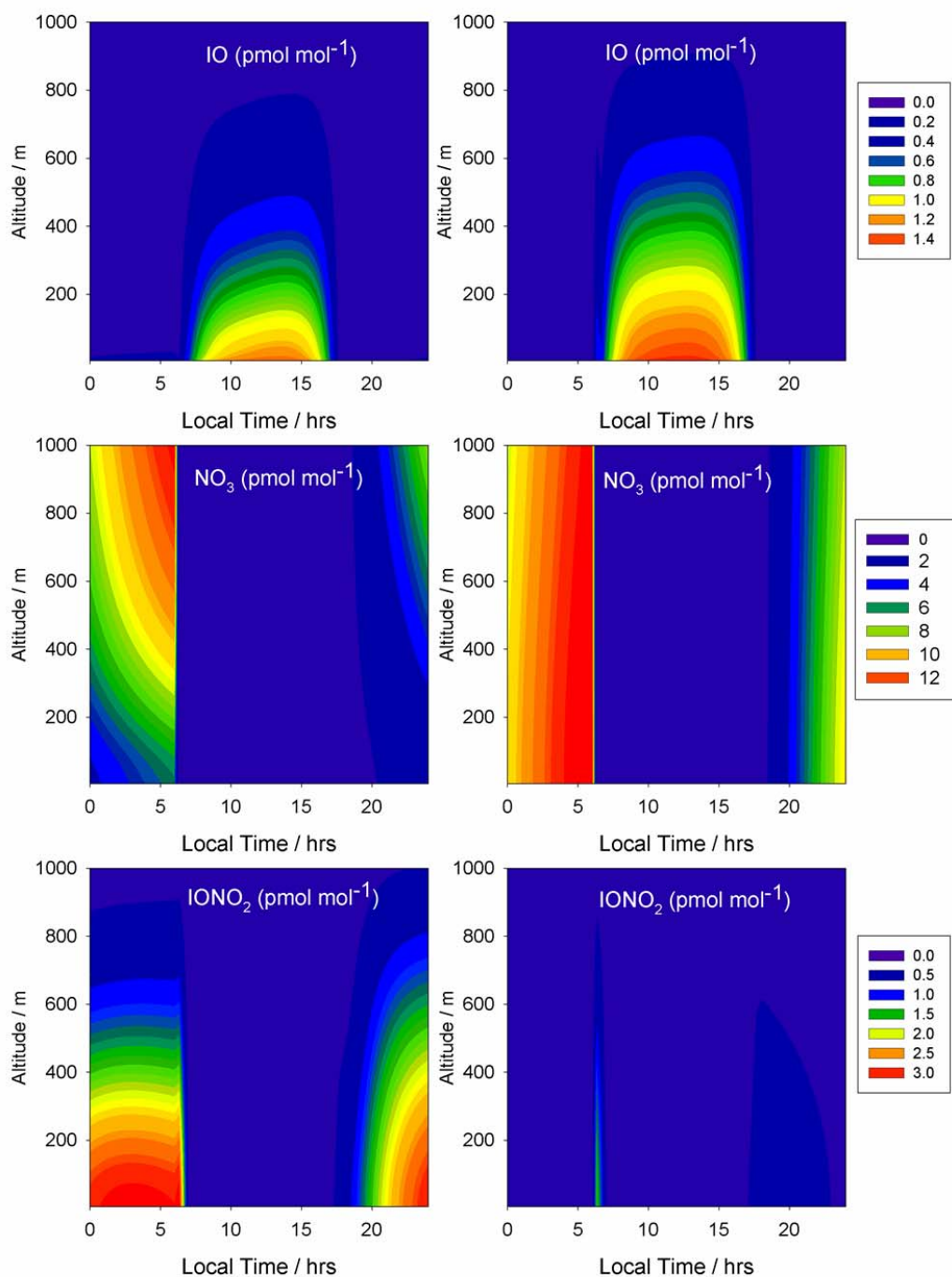
Figure 5. THAMO modeled diurnal variation of IO, NO_3 and the $IONO_2$. The right hand panels are from scenario 1, which do not include night time reactions of HOI and I_2 with NO_3, while the left hand panels include the reactions in scenario 2.
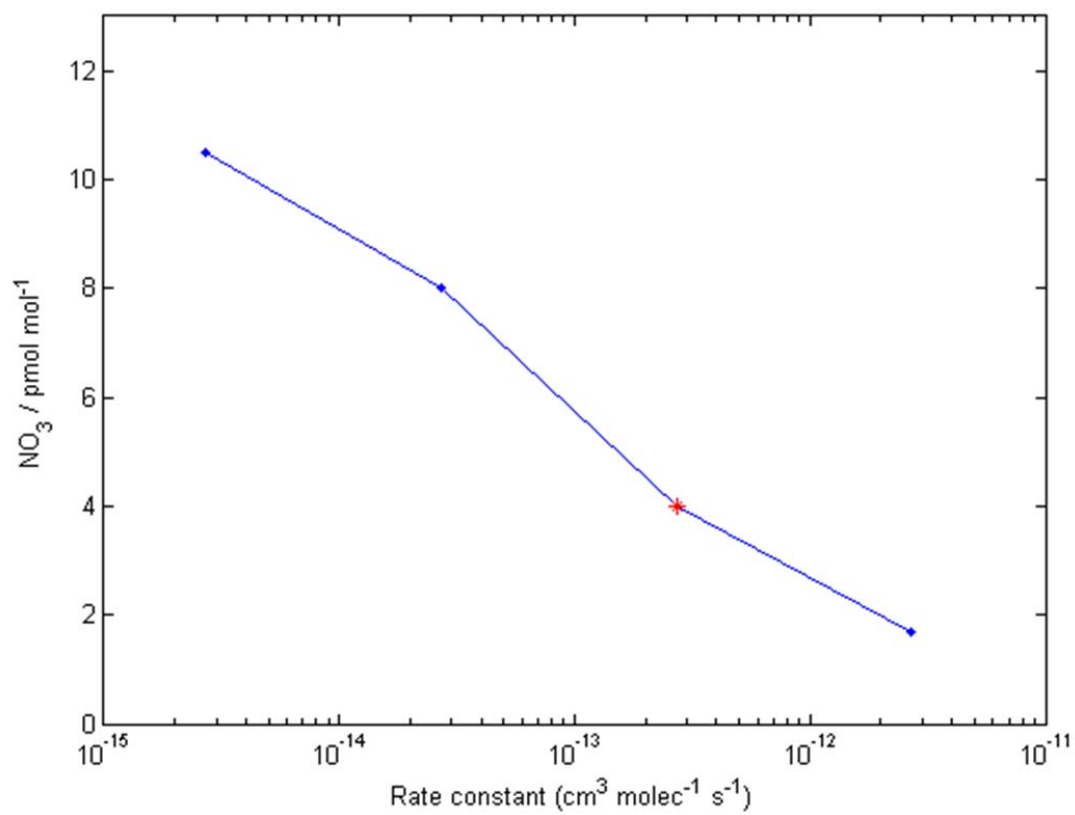
2 **Figure 6**. Sensitivity run showing the effect of the uncertainty in the rate constant estimation on

3 the reduction of NO$_3$ peak nighttime concentration at the surface - the red point is the theoretical

4 estimate.
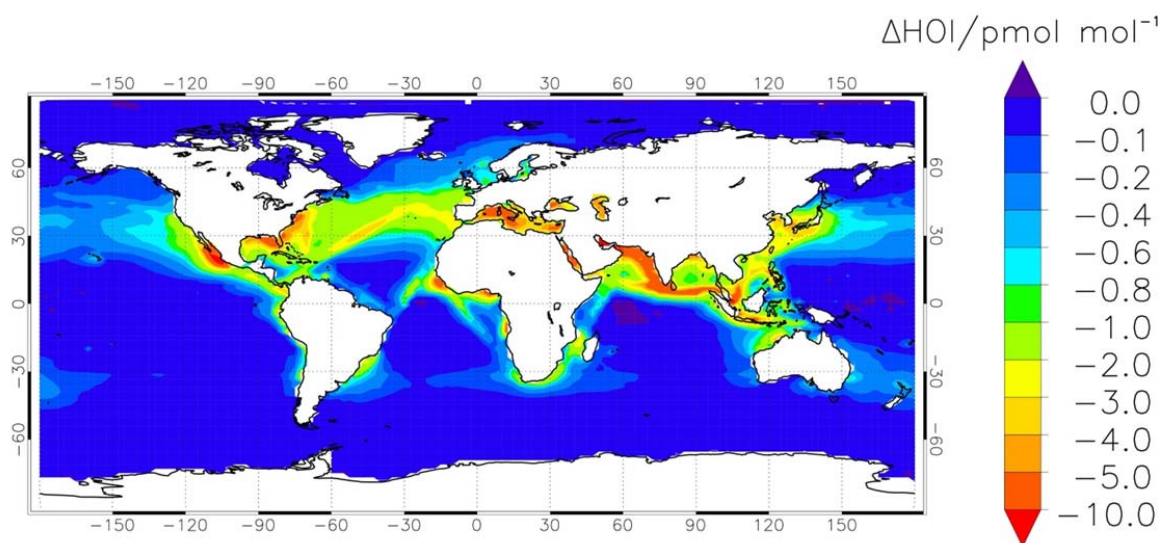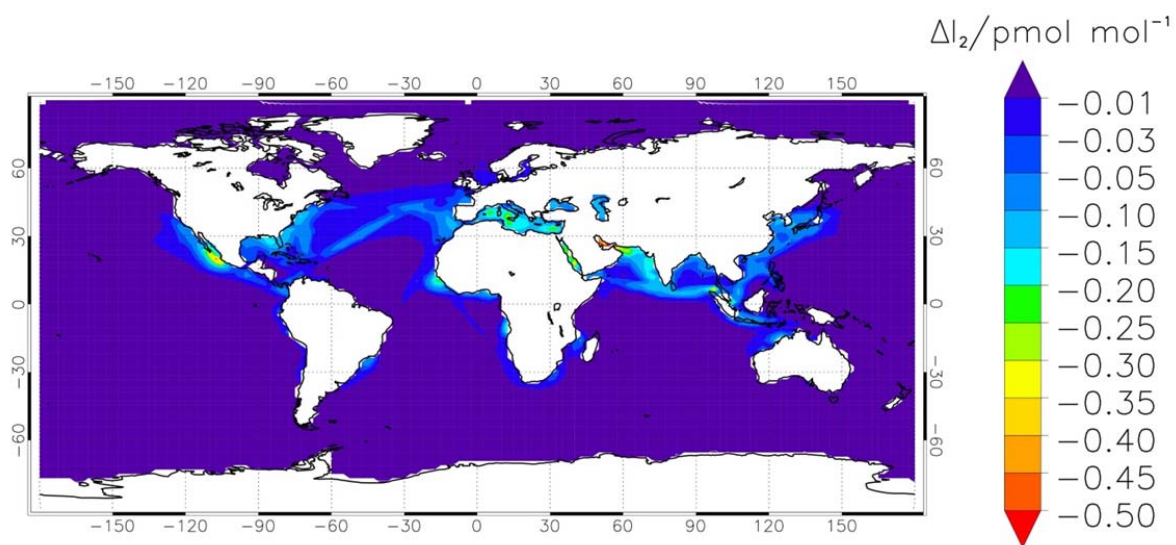
Figure 7. Modelled annual average of HOI (a) and I_2 (b) during night time (from 0:00 to 1:00 LT) at the surface level. The panels show the difference in volume mixing ratio between the simulations with and without reactions (1) and (4).
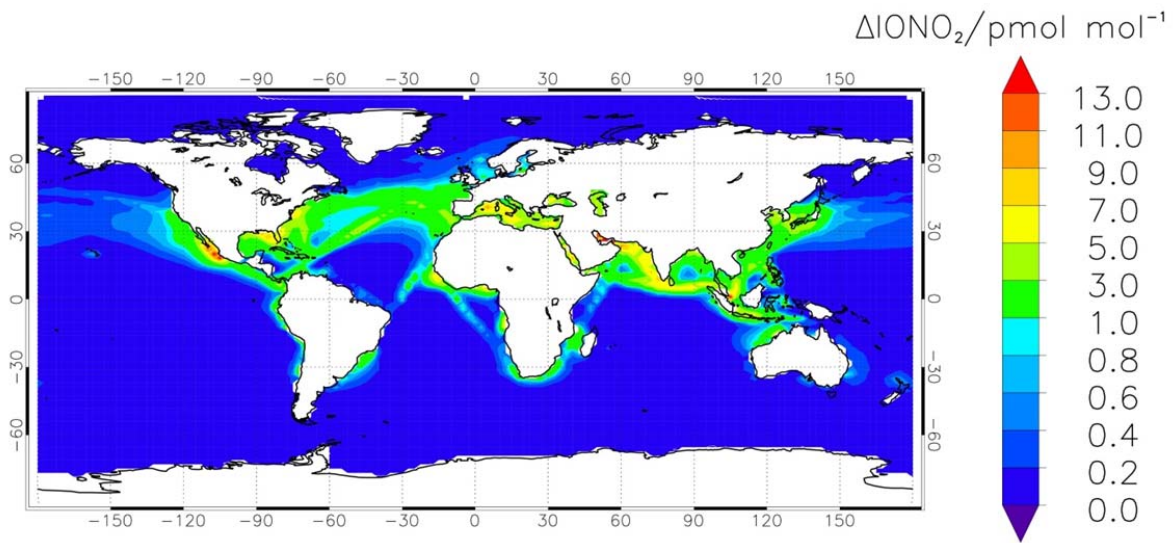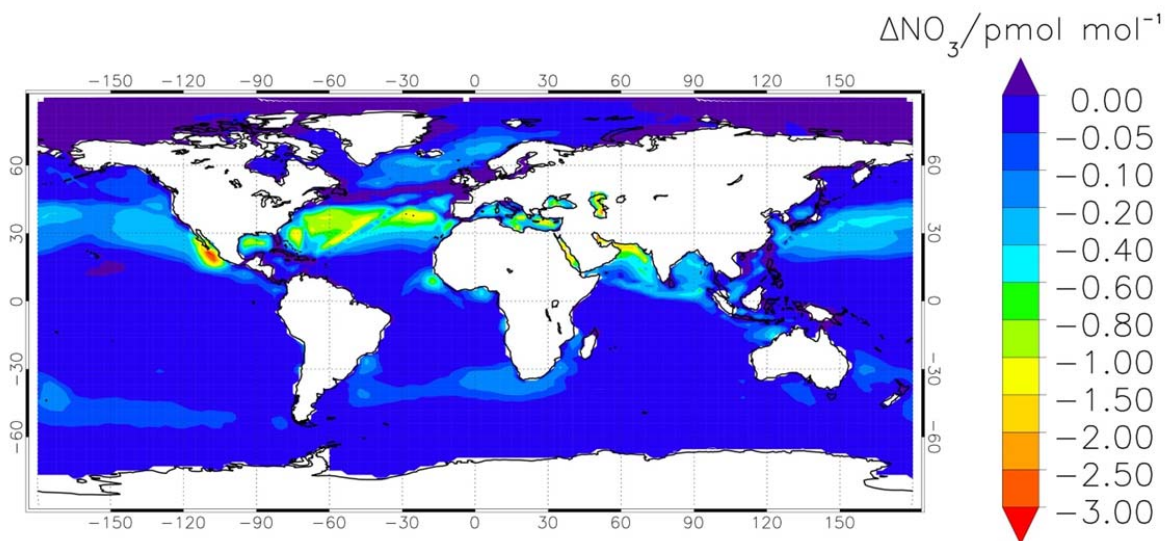
Figure 8. Modelled annual average of $IONO_2$ (a) and NO_3 (b) during night time (from 0:00 to 1:00 LT) at the surface level, as the difference in volume mixing ratio between the simulations with and without reactions (1) and (4).
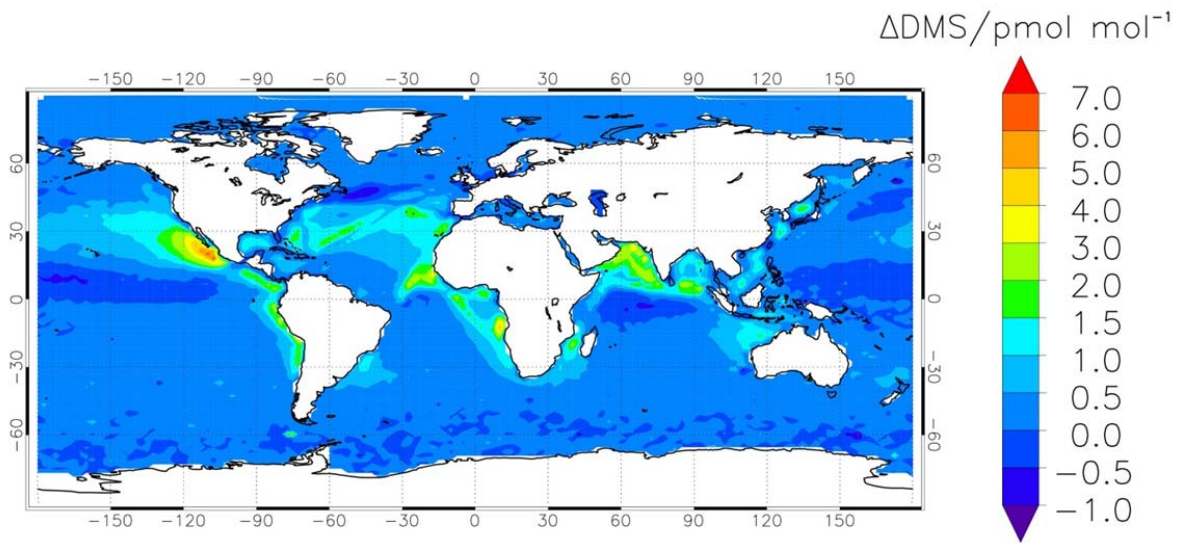
2 **Figure 9**. Increase in the DMS levels during night time (from 0:00 to 1:00 LT) at the surface
3 level due to the inclusion of the reactions R1 and R4 in CAM-Chem.
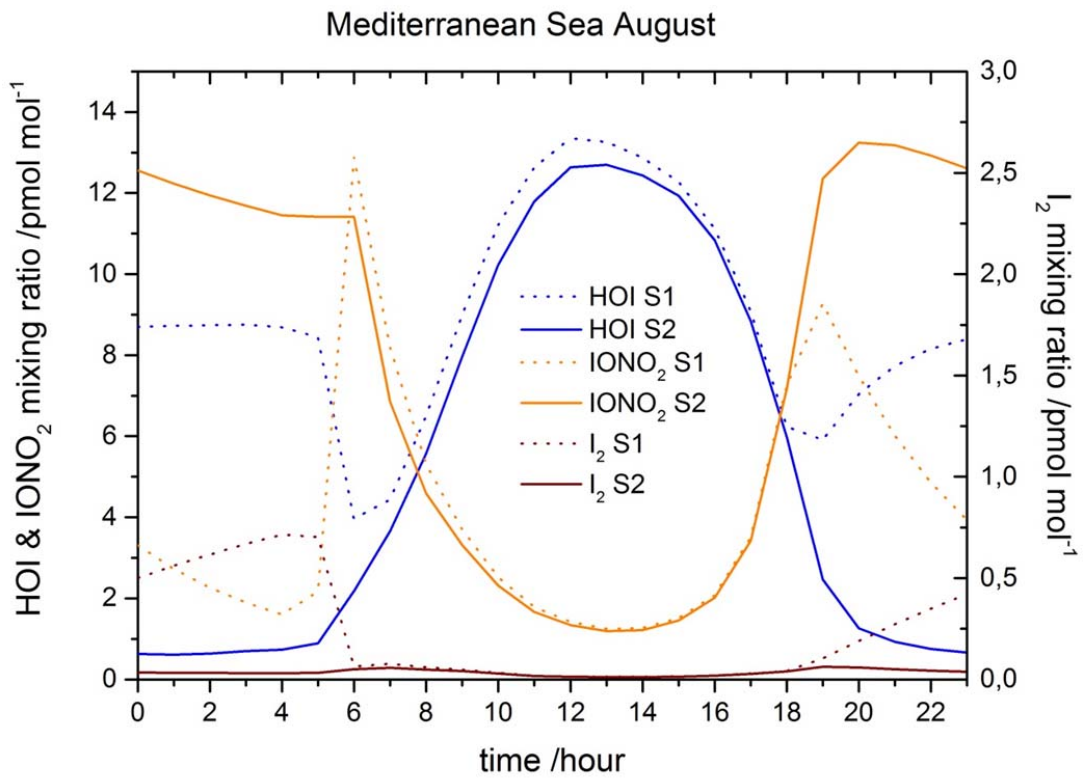
13 **Figure 10**. Hourly averaged concentration of HOI, IONO$_2$ and I$_2$ in the Mediterranean Sea at the
14 surface level (lon:10º→20ºE, lat:33º→40ºN)
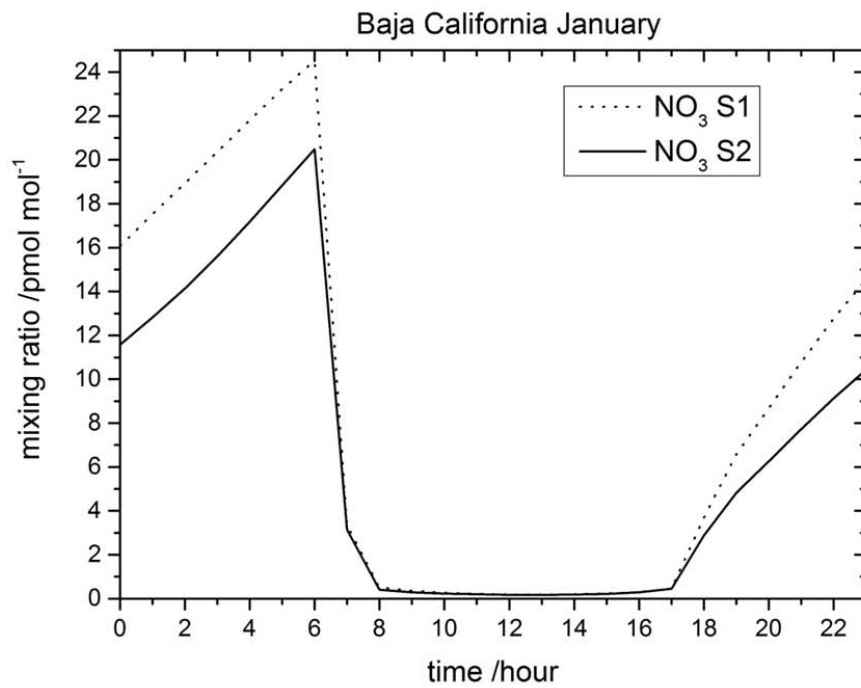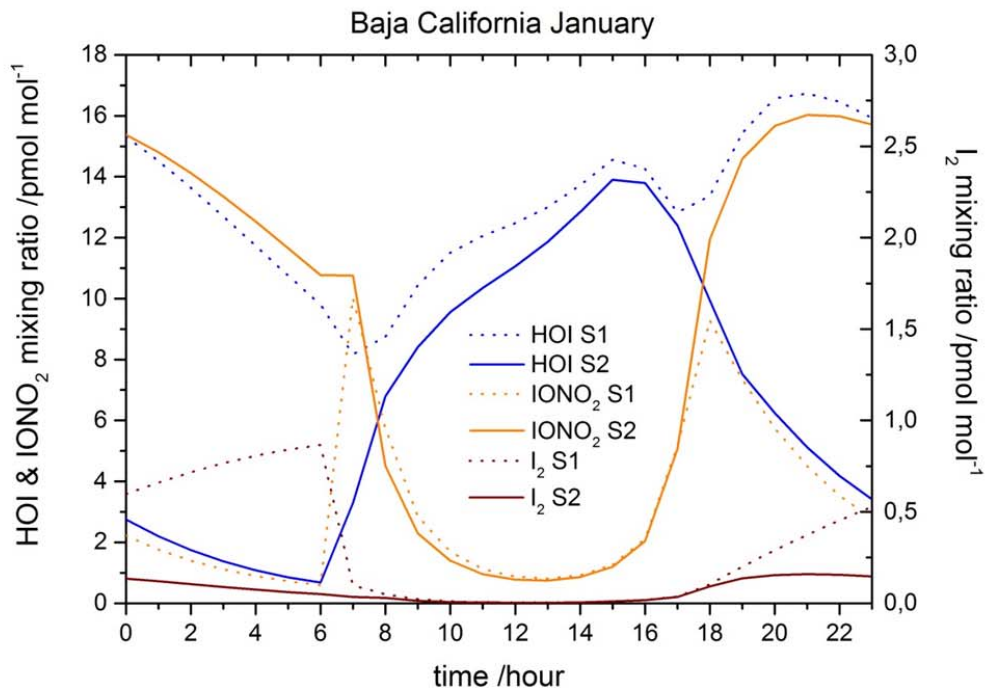
Figure 11. Hourly averaged concentration of HOI, IONO$_2$ and I$_2$ (upper panel) and NO$_3$ (bottom panel) in the Pacific Ocean at the south of Baja California peninsula at the surface level (lon: -110º→-106ºE, lat:16º→23ºN)